Archives of Civil and Mechanical Engineering (2024) 24:84
https://doi.org/10.1007/s43452-024-00882-0

ORIGINAL ARTICLE

Effect of olive-pruning fibres as reinforcements of alkali-activated cements based on electric arc furnace slag and biomass bottom ash

M. A. Gómez-Casero[1,2] · P. J. Sánchez-Soto[3] · E. Castro[1,2] · D. Eliche-Quesada[1,2]

Received: 14 August 2023 / Revised: 9 December 2023 / Accepted: 1 February 2024 / Published online: 18 March 2024

Abstract

In this work, alkali-activated composites using electric arc furnace slag (50 wt%) and biomass bottom ash (50 wt%) were manufactured, adding olive-pruning fibres as reinforcement. The objective of adding fibres is to improve the flexural strength of composites, as well as to prevent the expansion of cracks as a result of shrinkage. For this reason, composites reinforced with olive-pruning fibres (0.5–2 wt%) untreated and treated with three different solutions to improve matrix–fibre adhesion were manufactured. Treatments developed over fibres were a 10 wt% Na_2SiO_3 solution, 3 wt% $CaCl_2$ solution and 5 wt% NaOH solution. Mechanical properties, physical properties, thermal properties and the microstructure of composites by Fourier transform infrared spectroscopy (FTIR), X-ray diffraction (XRD) and scanning electron microscopy (SEM) were studied to demonstrate the improvement. Alkaline treatment degraded fibre surface, increasing the matrix–fibre adhesion, and as a consequence, flexural strength increased up to 20% at 90 days of curing. Optimal results were obtained with composites reinforced with 1 wt% of olive-pruning fibre treated by a 10 wt% Na_2SiO_3 solution. Higher quantity of olive-pruning fibre leads to local agglomeration, which weakens the matrix–fibre adhesion. The effect on the compressive strength is less evident, since the addition of fibres produces an admissible decrease (between 0 and 9% using 0.5 or 1 wt% of fibres), except in composites that use olive pruning treated with 10 wt% Na_2SiO_3 solution, where values remain stable, similar or better to control paste. A greater ductility of the matrix in all composites was observed. Furthermore, the alkali-activated cement matrix was bonded to olive-pruning fibre better than untreated fibre, as it is shown in SEM images. Thus, the results showed that olive-pruning fibres could be used as reinforcement in the manufacturing of alkali-activated materials when they are treated with alkali solutions.

Keywords Alkali-activated cements · Fibre treatment · Natural fibres · Electric arc furnace slag · Biomass bottom ash

Abbreviations

ATR–FTIR	Attenuated total reflectance–Fourier transform infrared spectroscopy
BBA	Biomass bottom ash
C	3 wt% calcium chloride solution treatment
C–(A)–S–H	Calcium–(aluminium)–silicate–hydrated gel
(C,K)–(A)–S–H	Calcium–potassium (aluminium)–silicate–hydrated hybrid gel
EAFS	Electric arc furnace slag
F/C	Flexural-to-compressive ratio
K–(A)–S–H	Potassium–(aluminium)–silicate–hydrated gel
M	5 wt% mercerization treatment
SEM–EDS	Scanning electron microscopy–energy-dispersive X-ray spectroscopy
Si	10 wt% sodium silicate solution treatment
UT	Untreatment
XRD	X-ray diffraction
XRF	X-ray fluorescence
wt	Weight

✉ M. A. Gómez-Casero
magomez@ujaen.es

[1] Department of Chemical, Environmental and Materials Engineering, Higher Polytechnic School of Jaén, University of Jaén, 23071 Jaén, Andalucía, Spain

[2] Center for Advanced Studies in Earth Sciences, Energy and Environment (CEACTEMA), University of Jaén, Campus Las Lagunillas, s/n, 23071 Jaén, Spain

[3] Joint Center of the Spanish National Research Council (CSIC), Institute of Materials Science of Sevilla (IMCS), University of Sevilla, 41092 Sevilla, Spain

1 Introduction

Alkali-activated materials have been extensively studied. It has been demonstrated that it is possible to produce green cement from different sources of wastes or natural minerals [1]. Natural minerals such as clays or zeolites [2], as well as industrial by-products, metallurgical wastes (slags) and ashes from biomass (fly or bottom), have been used [3, 4]. These materials have developed good compressive strength, but not so good flexural strength [5]. For this reason, several studies have emerged analysing different ways to reinforce the mechanical properties of these materials. These works are focused on the reinforcement of cements or alkali-activated cements with fibres. The reinforcement with fibres improve the flexural strength, toughness and impact resistance, as well as provide greater acoustic and thermal insulation capacity [6], since fibres help to counteract effects produced by the appearance of cracks in the matrix [7]. Fibres can be from synthetic or natural origin [8].

Synthetic fibres are man-made and they have been used in other composites. There are different types of synthetic fibres: inorganic, organic and steel fibres [9]. Due to the increased interest in creating more environmentally friendly materials, natural fibres are being studied [10]. Natural fibres can be classified as animal, mineral and plant fibres [11], and these last like non-wood or wood fibres [12], depending on the composition and their origin. In fact, chemical composition of plant fibres affects their physical and mechanical properties, which are composed of lignin, cellulose, hemicellulose and other substances [8]. Plant fibres are economic and renewable and they have great availability and low energy consumption in their production, and for this reason they are being considered to replace synthetic fibres available in the market [13].

Natural fibres can be used in treated or untreated form. In treated form, fibres can improve the behaviour front tensile strength, shrinkage effects, ductility, among others. If an alkali treatment is carried out on fibres, they could resist alkaline hydrolysis due to the alkali environment of alkali-activated cements [8, 14]. There are different treatment forms developed over fibres, of which the most known are as follows:

- Hornification: this process consists of wet and dry cycles, obtaining fibres with more stability and lower water absorption capacity [12, 15];
- Mercerization: this process includes immersing fibres in an alkaline solution ($Ca(OH)_2$, NaOH or a combination of NaOH and silane) for a set time, improving adhesion between fibre and matrix and as a consequence mechanical properties [8, 16, 17];
- Silane treatment: this process involves immersing fibres in a silane solution, modifying fibre surfaces to obtain better mechanical strength and lower water absorption capacity [18, 19];
- Hydrothermal treatment: here, fibres are immersed in boiling water, thus its crystallinity is increased [20].
- Acetylation treatment: this treatment produces a chemical reaction introducing acetyl function group into natural fibres and it is usually carried out after other treatments such as mercerization [21]. Here, hydrophobic fibres are achieved, reducing mineralization [20].
- Other chemical surface treatments: benzoylation and peroxide. They improve the adherence between fibres and matrix and they reduce the hydrophilicity [22].
- Mechanical refining treatment: it usually develops after alkali treatment [23].
- Physical methods: Stretching, plasma treatment or electric discharge modifies fibre surfaces, but they do not change chemical compositions, changing the properties of fibres [24].
- Or a combination between them [18].

Numerous studies have been conducted on both treated and untreated natural fibres. For instance, Souza et al. [8] utilized sisal fibres treated with varying percentages of NaOH, followed by washing with water or acetic acid. The results demonstrated that the NaOH treatment enhanced the tensile strength of the fibres, as a consequence of the reduction in their hemicellulose and lignin composition. Li et al. [25] treated bamboo fibres with NaOH, enhancing the toughness and flexural strength of the reinforced cements. Banjo et al. [26] employed combined alkali treatments with microwaves on bamboo fibres, improving fibre behaviour when microwaves were applied along with a mercerization treatment. Dhasindrakrishna et al. [27] treated hemp fibres with alkali, which enhanced mechanical properties even at temperatures of 100 and 200 °C, but did not achieve improvement after exposure to 400 and 800 °C. Fei et al. [28] used water glass to modify the surface of bamboo fibres, which enhanced fibre–matrix interaction and the flexural strength of the composites.

In this study, electric arc furnace slag (EAFS) and biomass bottom ash (BBA) have been used as precursors, according to previous results [29]. EAFS is made up of SiO_2, CaO and Fe_2O_3 [30], for steel-making process. The chemical composition of BBA depends on the origin of biomass. Ashes used in the present study are obtained from a biomass power plant that manufactures biomass from olive and forest pruning. The novelty of the study lies in the use of olive-pruning fibres as reinforcement of natural fibres, not previously studied as reinforcement, untreated and subjected to different chemical treatments of alkaline activation cements based on 50 wt% EAFS-50 wt% BBA.

Olive-pruning fibres were treated with different solutions: 10 wt% Na_2SiO_3, 3 wt% $CaCl_2$ and 5 wt% NaOH. The effect of reinforcement of the fibres in the binder matrix to increase the flexural strength and ductility has been studied, studying the effect on the physical, mechanical and thermal properties caused by the reinforcement in the matrix of the alkali-activated cement as a function of the wt% of fibre incorporated (0.5–2 wt%) and the chemical treatment used.

2 Materials and methods

2.1 Raw materials

Precursors used were supplied by Siderúrgica Sevillana S.A., located in Alcalá de Guadaira (Sevilla, Spain) in the case of slags, and biomass bottom ashes were provided by Aldebarán Energía del Guadalquivir, sited in Andújar (Jaén, Spain). Electric arc furnace slag (EAFS) was obtained from the process of refining in steel production using an electric arc furnace. Biomass bottom ash (BBA) is a waste obtained from a power plant which uses olive and forest pruning and olive pomace to produce electricity from thermal energy.

Both raw materials were crushed in a ball mill until a particle size of less than 0.1 mm was obtained. The particle size distribution is shown in Fig. 1, and it was determined by laser diffractometer. Both materials had similar size distribution. They present a homogeneous particle distribution and the main particle size (d_{50}) for both precursors was 21.8 µm and 29.9 µm, for EAFS and BBA, respectively.

The chemical composition of raw materials obtained by X-ray fluorescence (XRF) is shown in Table 1. The XRF results show that the main components of BBA are SiO_2 (46.10%), Al_2O_3 (12.04%) and CaO (19.65%). In the case of EAFS, the percentage of major component is 30.89% of CaO and 24.16% of Fe_2O_3, with significant quantity of SiO_2 (17.29%) and Al_2O_3 (10.71%).

SEM was performed to investigate the morphological properties and microstructure of precursors (Fig. 2). Both raw materials exhibited a heterogeneous particle size distribution. The slag particles were rough, presenting slightly rounded particles and angular particles, while the ashes contained spherical glassy particles, as well as angular particles and a small amount of unburnt carbon (dispersed porous particles).

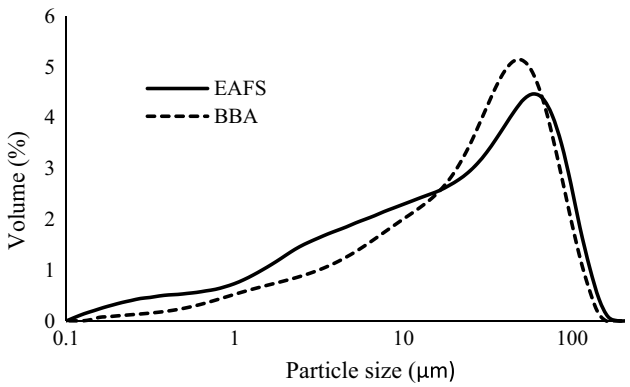

Fig. 1 Particle size distribution of precursors

Table 1 Chemical composition of raw materials

	SiO_2	Al_2O_3	CaO	Fe_2O_3	K_2O	Na_2O	MnO	MgO	SO_3	LOI
BBA	46.10	12.04	19.65	4.78	4.59	0.78	0.09	3.71	0.41	5.58
EAFS	17.29	10.71	30.89	24.16	0.03	0.16	5.68	2.63	0.28	5.39

2.2 Fibre as reinforcement

Fibres used as reinforcement were obtained from olive pruning (Fig. 3). They were crushed until obtaining the range retained on the sieve between 0.125 and 0.250 mm. Three chemical treatments were performed on the fibres to improve the mechanical properties of binders. Treatments consisted of immersing fibres in a chemical solution for 60 min under rapid stirring, with a relation of 1/50 (fibre/solution). Then they were drained and cleaned with distilled water up to neutral pH. Fibres were dried in an oven. They were stored in closed containers until manufacture day. The treatment solutions used were: 10 wt% Na_2SiO_3, 3 wt% $CaCl_2$ and 5 wt% NaOH (process known as mercerization) in distilled water. These solutions are considered economical modifiers by other authors [28].

Fibres were added in different proportions to reinforce binders: 0.5 wt%, 1 wt% and 2 wt%. The binders were designed as *X–Y*, except control paste that it was designed as *Control*, where *X* is the treatment developed on the fibres and *Y* is the content of fibres in the binder, being *UT = untreatment*, *Si = fibres treated with 10 wt% sodium silicate solution*, *C = 3 wt% calcium chloride solution* and *M = mercerization* (e.g. C-1, binders with 1 wt% of fibre treatment with 3 wt% $CaCl_2$).

The chemical composition of untreated and treated fibres was determined according to Padilla-Gascón et al. [31], who followed a modified process from Sluiter et al. [32]. Two extractions were carried out before, first with water and then ethanol, for extractives, by Soxhlet method.

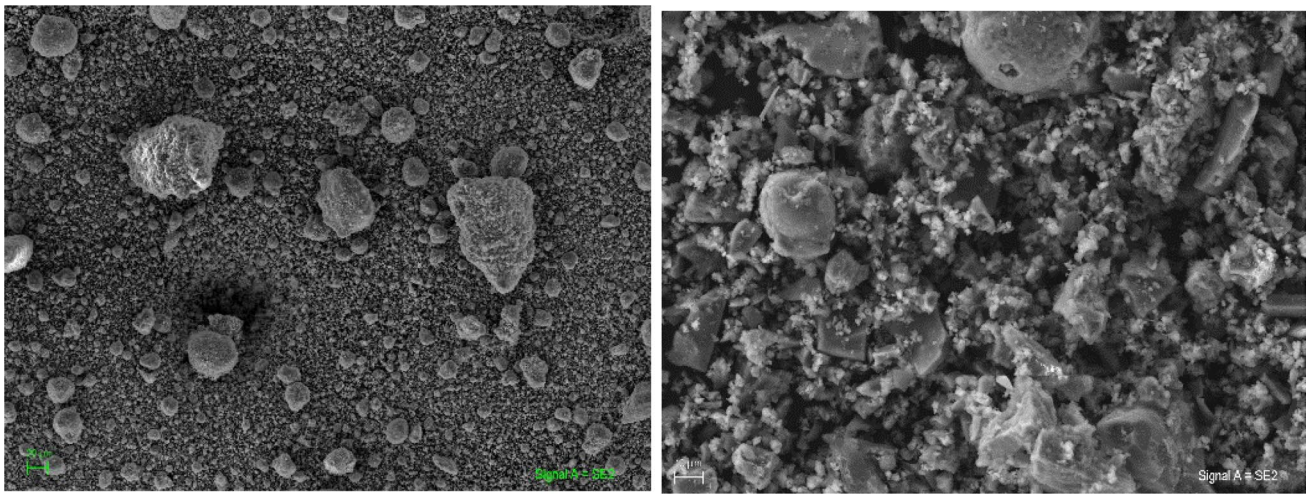

Fig. 2 Precursors' SEM micrographs

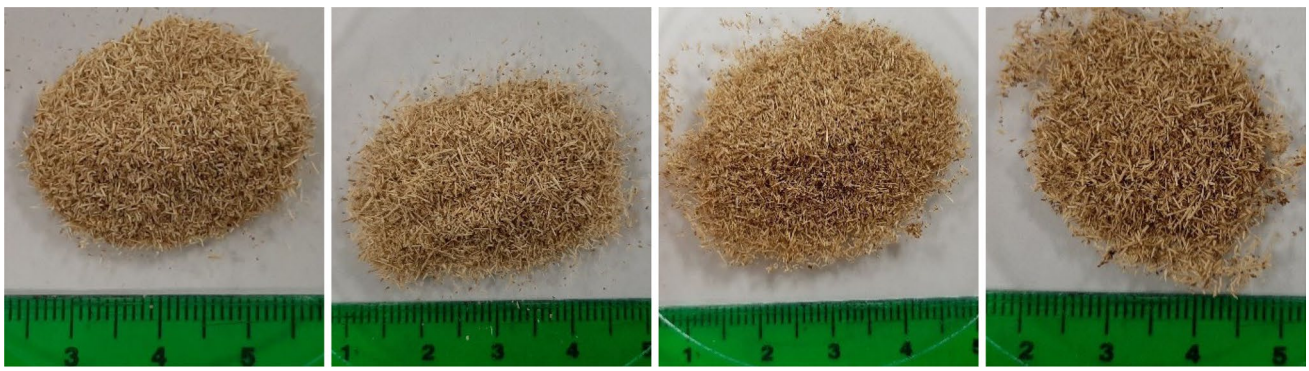

Fig. 3 Fibre images: **a** fibres untreated, **b** fibres treated with calcium chloride solution, **c** fibres treated by mercerization, **d** fibres treated with sodium silicate solution

2.3 Binder manufacturing

The proportion used in the manufacturing of binders was 50 wt% BBA and 50 wt% EAFS. This composition was obtained as the best proportion in previous works [29]. Fibres were added to the mixture of precursors.

The alkaline activator used was a mix of 50 wt% KOH (8 M) and 50 wt% K_2SiO_3. This activator was set following the results of previous works. KOH with 85% of purity was used and K_2SiO_3 was supplied with a composition by weight as follows: 7.5–8.7% K_2O, 19.5–21.8% SiO_2 and 69.5–73% H_2O. The Ms (SiO_2/K_2O) obtained was 0.89 and the liquid/binder ratio used was 0.6 for all specimens.

Binders were manufactured following the same sequence. Precursors and fibres were mixed in a planetary mixer for 90 s; subsequently, the activator solution was poured and the materials were mixed for 90 s. Then, the walls were drained with a scraper and the paste was mixed for 30 s more. After this process, the activated pastes were poured into two types of moulds: steel prismatic moulds (60 × 10 × 10 mm) and plastic cylindrical moulds (ϕ 55 mm). Moulds with fresh pastes were put on a flow table for 60 hits. The moulds were saved in a climatic chamber at 20 °C and 90% RH for 24 h and then they were demoulded. After that, they were stored in the climatic chamber at the same conditions until test day.

The physical and mechanical properties were obtained at 1, 7, 28 and 90 days of curing. The mechanical properties were obtained following UNE-EN 1015–11:2000/A1:2007 [33] and physical properties according to UNE-EN 1015–10 [34]. Prismatic samples were tested for this purpose. Thermal conductivity was determined at 28 days of curing, using a heat flow metre machine according to ISO 8302 [35] over cylindrical samples. A flow test was carried out over fresh composites following ASTM C-1437 standard [36].

Besides, all fibres and specimens were analysed by ATR–FTIR, and the selected samples were explored by XRD and scanning electron microscopy–energy-dispersive X-ray spectroscopy (SEM–EDS).

3 Results and discussion

3.1 Workability of fresh pastes

The workability results of fresh pastes are shown in Fig. 4. These values were determined by comparison with the control sample, which obtained a spread diameter of 81.75 mm. The workability of samples incorporating fibres decreased with the increase in the quantity of added fibres. The decrease was minor or barely noticeable when 0.5 wt% of any fibre was added. The loss of fluidity in the mixture is attributed to the rough surface of the fibres, increasing internal resistance and friction [37].

However, as the percentage of fibres increased, the behaviour varied depending on the type of fibre used, with a greater loss of workability observed for fibres treated with silicate and NaOH. The reason is the rougher surface of fibres treated with these solutions, which negatively affects the workability of composites in their fresh state compared to the other fibres [38, 39].

3.2 Mechanical properties

The effect of olive pomace fibre as reinforcement on the flexural strength of alkali-activated cements for different fibre contents is presented in Fig. 5. The results show that olive pruning before and after treatment does not always improve flexural strength compared with control alkali-activated cements: 2.6 and 3.4 after 28 and 90 days of curing. However, treated fibres improve flexural strength with respect to untreated fibres. This is because the treatment improves adhesion and fibres can bond more tightly with the matrix of alkali-activated cements [40–42]. The best value was obtained using 1 wt% of fibre treatment with Na_2SiO_3, 3.9 MPa and 4.2 MPa at 28 days and 90 days of curing, respectively, which represents an improvement of 20.1% at

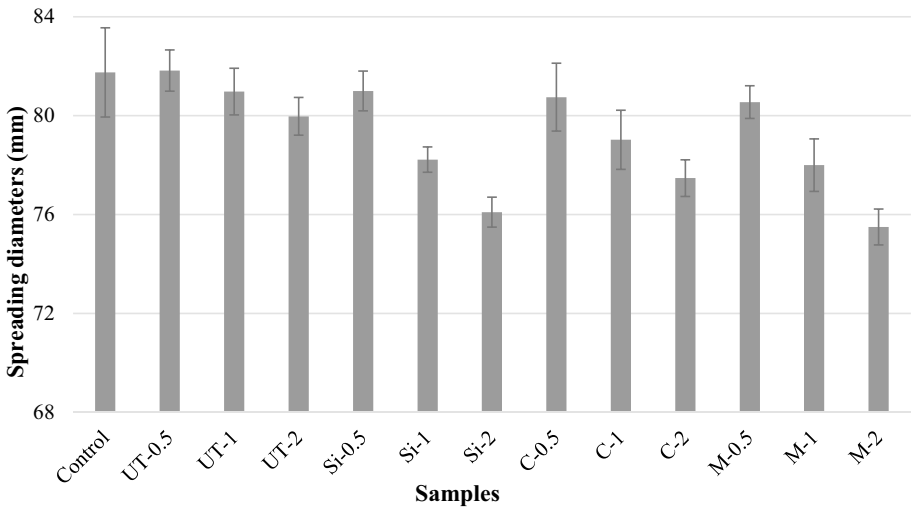

Fig. 4 Spreading diameters of fresh composites

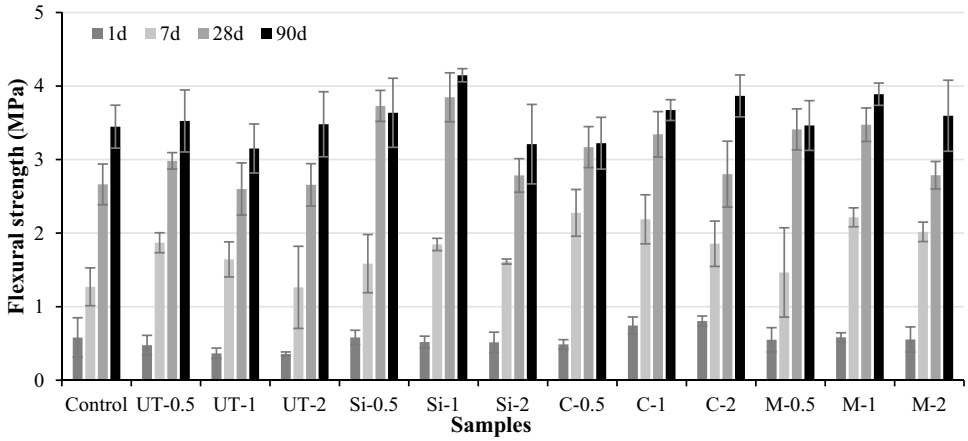

Fig. 5 Flexural strength as a function of reinforcement used and curing time

90 days of curing, with respect to control paste, and more than 20% with respect to untreated fibre pastes. This value is not far from that obtained in the literature at 28 days[10]. Si-0.5 obtained great values, near to Si-1. Other satisfactory results were obtained for C-1, C-2 and M-1, with best values than control pastes. The rest of specimens developed better strength than that of control pastes at 90 days of curing, except UT-1, Si-2 and C-0.5. The treatment allows a higher transfer of the matrix to fibres, which improves flexural strength. Optimal values of flexural strength were obtained when 1 wt% of treatment fibres was added. Thus, this fibre content allows the optimal transfer of tensions from matrix to olive fibres, which leads to an improvement in flexural strength. These results are according to literature, where optimal amount varies between 0.5 and 2 wt% [43, 44]. Possibly, when increasing fibre content, the matrices and fibres are mixed unequally, producing a local agglomeration, which degrades interfacial adhesion and weakens the union between the matrices and fibres. In addition, these agglomerations can act as tension concentrators and reduce the flexural strength [45, 46].

Regarding the influence of curing time, comparing values at 7 days and 28 days of curing, it is possible to see an improvement in flexural strength. However, the increase of curing time up to 90 days did not significantly increase flexural strength. This is due to the greater amount of C–(A)–S–H gel and geopolymeric K–(A)–S–H gel or hybrid (C,K)–A–S–H gel formed during alkali activation process, producing an increase in flexural strength for composite reinforcement with treated and untreated fibres. As a result of the lower adhesion of untreated fibres, their improvement was less evident. Therefore, the addition of adequate amounts of olive-pruning fibres treated in alkaline medium can slightly improve the tenacity of alkali-activated cements.

In compressive strength test, the matrix is more important than fibre reinforcements; for this reason, the effects of reinforcement are less evident. In Fig. 6, the stress–strain curves of control composite and those containing 1 wt% of fibres are shown. The stress–strain curves show a high slope line and a lineal shape due to the capacity of matrix and the transfer of stress from matrix to fibres, and it depends on the reinforcement properties and the matrix adhesion. Composites reinforced with fibres show similar compressive strength values to those of control paste, although a higher ductility is observed when fibres are introduced.

The compressive strength results are shown in Fig. 7. The values decrease when the amount of fibres is increased, between 0 and 9% using 0.5 or 1 wt% of fibres. When composites were tested for compressive strength, the strength was developed by matrix of alkali-activated cement. In general, the addition of fibres increases the porosity of composites and maximum stress with respect to matrix can decrease. As mentioned in Sect. 3.8, samples with a higher fibre content (2 wt%) develop fissures that will impact compressive

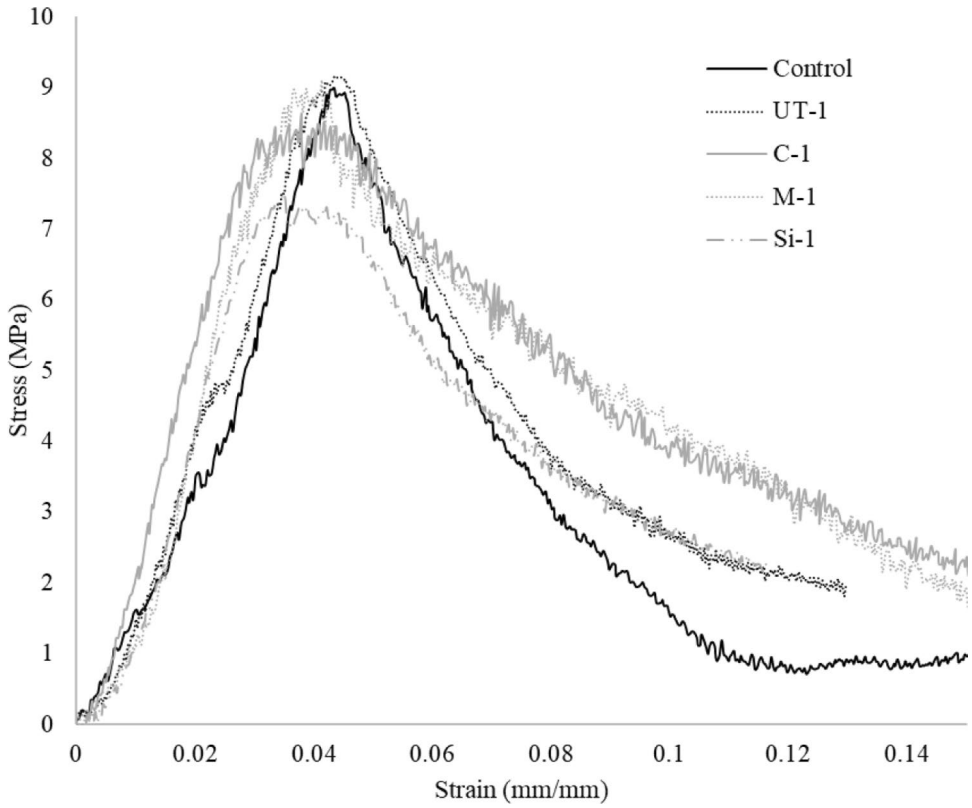

Fig. 6 Stress–strain curves of control composites and reinforced composites

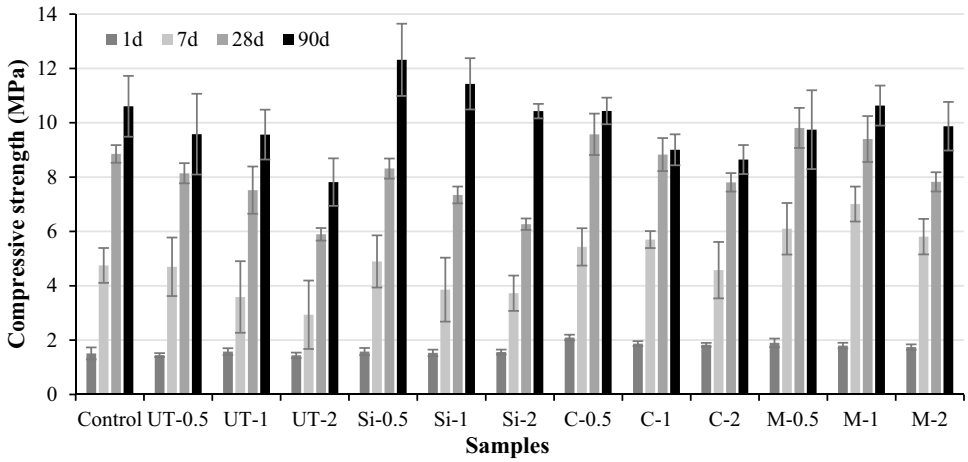

Fig. 7 Compressive strength as a function of reinforcement used and curing time

strength. On the contrary, close to the fracture point, fibres have a union effect that increases the ductility of composite, increasing the deformation values. Best values at 90 days were obtained by Si-0.5 (12.32 MPa) and Si-1 (11.43 MPa), improving values with respect to control paste, between 7.8 and 16.1%.

C-0.5 (10.44 MPa) and M-1 (10.63 MPa) equalized the compressive strength values of control paste (10.6 MPa). In the case of untreated fibres, composites did not increase compressive strength results, obtaining same UT-0.5 and UT-1 values (9.6 MPa). The improvement in compressive strength, compared to the control paste, is attributed to the good dispersion of the fibres throughout the matrix [43, 44]. This helps in increasing matrix/fibre interaction. In fact, best results are obtained when fibres are treated.

The loss of compressive strength in Si or M specimens with respect to composites with less amount of fibres can be considered admissible, because they obtained higher or similar values than those of control composites. Besides, all composites obtained best *F*/*C* ratio (flexural-to-compressive ratio, Fig. 8) compared with control composites, with Si-1 being the best specimen, which confirms that the optimal composites were pastes with 1 wt% of fibres treated with sodium silicate. F/C ratio is related with better crack resistance [14]. In addition, 1 wt. % of fibres was the optimal amount of fibres to adding in composites improving *F*/*C* ratio in front to control composites. A higher or lower percentage led to a lower increase in mechanical strength [14].

3.3 Physical properties

The physical properties are presented in Fig. 9. Bulk density decreased when the amount of fibres increased. The loss of bulk density can be attributed to the lower density of fibres. In addition, the decrease in bulk density is affected because the fibres are agglomerated during the mixing process and occupy spaces full of water that are emptied in the curing process, becoming porous in the matrix [47]. Furthermore, the increase of fibre content caused an increase in the viscosity of the matrix (see Sect. 3.1), which favoured the introduction of residual air bubbles in the mixture and during the pouring of the paste into moulds. These bubbles gave rise to a greater amount of microvoids and less dispersion of fibres.

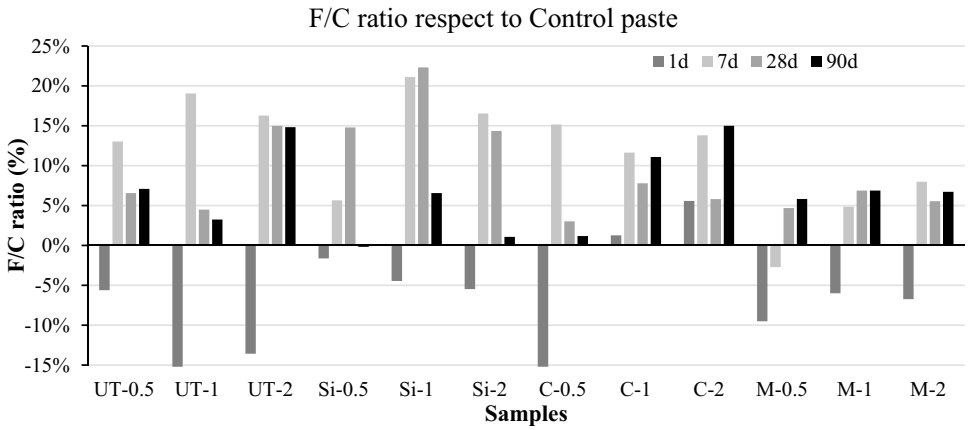

Fig. 8 Flexural/compressive ratio with respect to control paste, as a function of reinforcement used and curing time

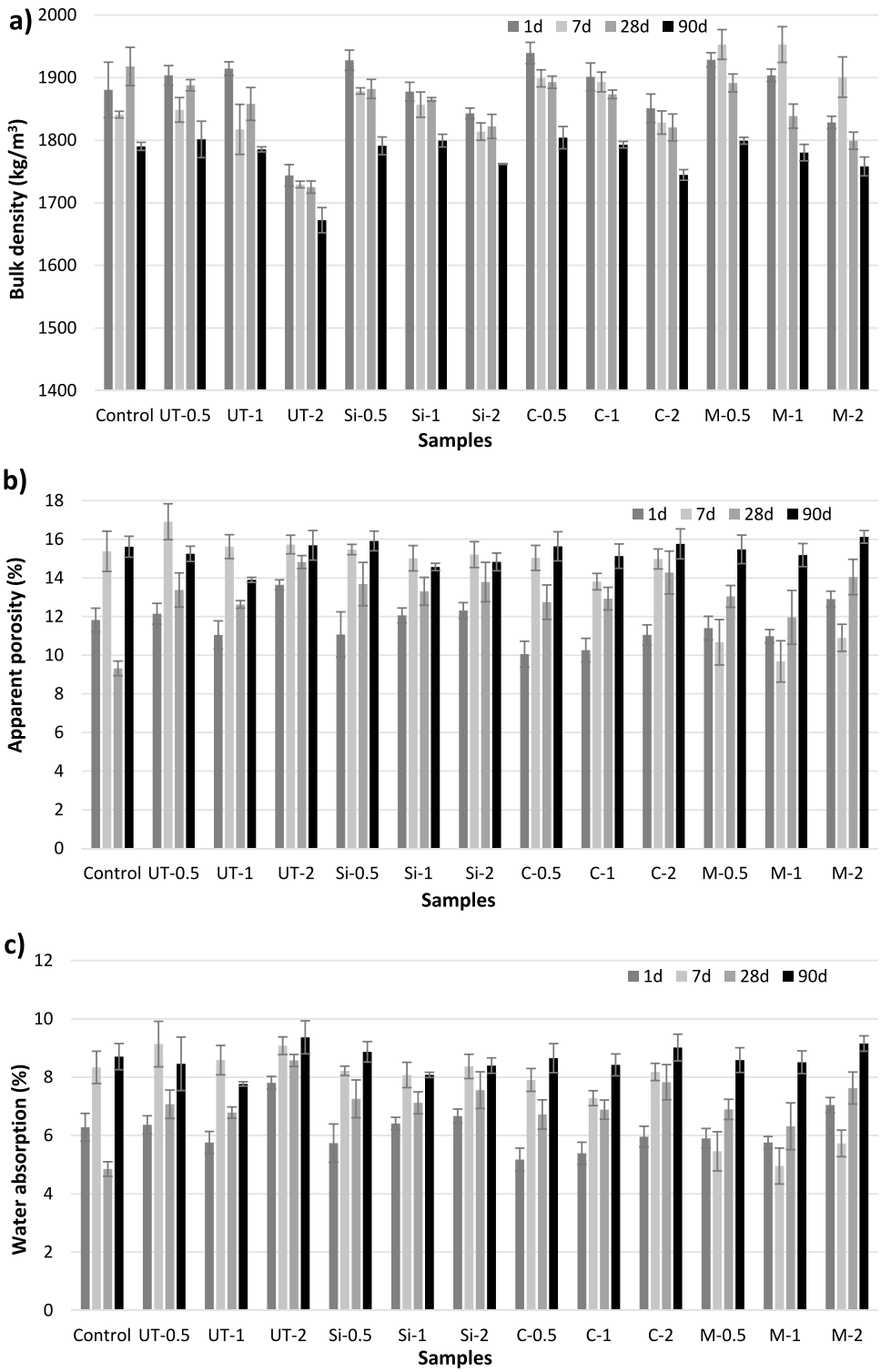

Fig. 9 Physical properties: **a** bulk density, **b** apparent porosity and **c** water absorption

For these reasons, at 28 days, the highest value of bulk density was found for control paste. If the values were compared at early ages, the trend is different. Probably due to excess of humidity of composites in fresh state, later geopolymerization and alkali activated processes, and the interaction of the fibres in these processes. Nevertheless, all samples decreased within the 5% margin established in the literature [48], with the exception of UT-2 (10.0% decreased) and C-2 (5.1% decreased). The greater the amount of fibres added, the greater the loss of bulk density, because the agglomeration of fibres produces intergranular pores that have negative effects on mechanical properties

[49]. Thus, samples with 2% of fibres have the lowest densities. However, it was observed that samples reinforced with untreated fibres obtained lower bulk densities than those of treated fibres. This is consistent with other studies [50]. This shows that the treatment of fibres helps in obtaining a lower decrease in bulk density, as discussed in the microstructural analysis (Sect. 3.8).

The apparent porosity and the water absorption are related properties. Both increase with the incorporation of fibres to the matrix. This behaviour is due to two reasons: fibre structure causes great absorption capacity (2.5 times their weight) and fibres create new pore structure in the matrix [48]. Fibres may tend to clump together during mixing, creating water-filled spaces that later become voids. Therefore, higher fibre content can increase the potential for fibre clumping, leading to an undesirable non-uniform microstructure [51]. Best apparent porosity and water absorption values were obtained for control paste and the worst values were obtained for UT-2.

3.4 Thermal conductivity

Thermal conductivity results at 28 days of curing are presented in Fig. 10. Thermal conductivity decreases with addition of fibres according to bulk density data [47, 52]. Control paste exhibited the highest value of thermal conductivity (0.80 W/mK). The decrease in conductivity values is associated with the presence of pores in the matrix. This is due to the low conductivity of air (0.026 W/mK) present in the pores [53].

As mentioned before, the porosity increases with the addition of fibres; thus, there is a higher air content, causing a decrease in the conductivity data. Depending on treatment used, the decrease was greater or less. Thus, higher decrease is found in samples reinforced with untreated fibres and fibres treated with NaOH (values between 0.54 and 0.70 W/mK and 0.53 and 0.67 W/mK, respectively), while fibres treated with $CaCl_2$ did not have significant changes (0.72–0.75 W/mK).

3.5 Fibre constituents

Fibre constituent result are shown in Table 2. The results reveal that untreated fibres contain a large amount of extracts (38.19 wt%), which are eliminated after treatments. In addition, treatments modified the composition of lignocellulosic material (cellulose, hemicellulose, lignin and others). The cellulosic content increased on applying any treatment, with the treatment with sodium silicate exhibiting the highest cellulosic content. This value agrees with the highest compressive strength sample. Alkaline treatments produced an increase in the tensile strength of the fibre, increasing the strength of the composite [54]. Non-cellulosic content decreased when fibres were treated by mercerization or with a sodium silicate solution. However, the hemicellulose content decreased when fibres were treated with a $CaCl_2$ solution, but their lignin content increased considerably. The lignin rise in these fibres could cause less geopolymerization, because according to other authors, this rise has a negative effect [55]. The removal of non-cellulosic content improved the matrix–fibre interaction, improving

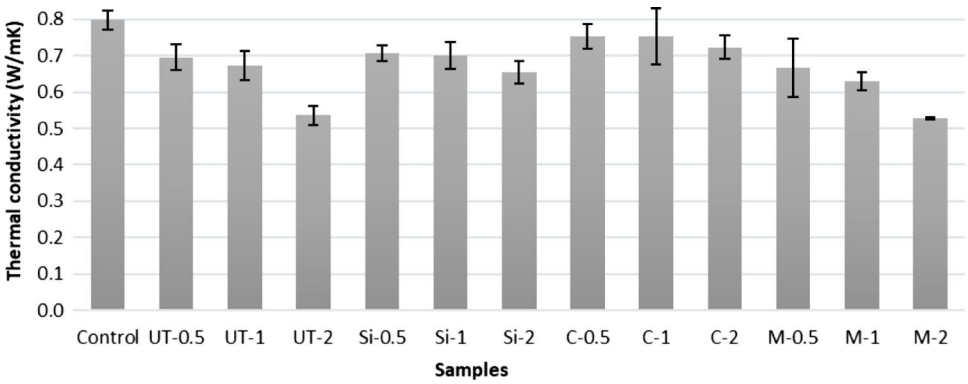

Fig. 10 Thermal conductivity at 28 days of curing

Table 2 Lignocellulosic composition of raw and treated olive-pruning fibres

Treatment	Cellulose	Hemicellulose	Lignin	Others	Moisture
UT (without extractives)	23.45	24.93	36.19	5.44	9.99
10% Na_2SiO_3	35.40	17.24	30.57	9.54	4.99
3% $CaCl_2$	26.19	3.94	53.02	10.13	6.72
5% NaOH	34.15	17.37	34.65	8.84	7.24

Values are expressed as a percentage of dry weight

mechanical properties [56]. Besides, there is another advantage when removing non-cellulosic compounds: the degradation over time of fibres in the matrix decrease, due to less content, because the amount that can be dissolved in the interstitial water decreases [48].

3.6 Functional group analysis

3.6.1 Raw materials

The manufactured raw materials and binders were analysed by attenuated total reflectance-Fourier transform infrared spectroscopy (ATR–FTIR) using a Bruker Vertex 70 equipment. Raw materials' spectrograms are shown in Fig. 11.

EAFS shows 1433, 972, 882, 672 and 512 cm^{-1} as the main bands, and for BBA 1383, 969, 858 and 442 cm^{-1} are the principal bands. Centred bands at 3577 and 2833 cm^{-1} are characteristic of the presence of O–H and C–H groups, respectively [57]. 1433 and 882 cm^{-1} for EAFS and 1383 and 858 cm^{-1} centred peaks are associated with CO_3^{-2} bond groups [29]. Bands centred at 972 and 969 cm^{-1}, for EAFS and BBA, respectively, are attributed to the asymmetric stretching vibration of Si–O–Si or Si–O–Al bonds (tetrahedral Si or Al) [58]. This difference between wavenumber is due to the different chemical composition, according to the XRF results, where ashes have high SiO_2 content.

Two bands at 784 and 699 cm^{-1} in BBA are attributed to the presence of quartz [59], as shown in the XRF. For EAFS, centred bands at 672 and 512 cm^{-1} are assigned to Si–O vibrations [60]. The band centred at 442 cm^{-1} in BBA is characteristic to the bending vibration of O–Si–O [61].

3.6.2 Fibre analysis

The FTIR spectra of untreated and treated olive-pruning fibres are presented in Fig. 12. Fibres analysed show a wide absorption band at 3000–3500 cm^{-1} assigned to cellulose and moisture of fibres, O–H stretching vibration [54, 62, 63]. At 2920 and 2852 cm^{-1} are presented tow bands associated with cellulose and hemicellulose, C–H stretching vibration [56, 64]. Hemicellulose is also detected at 1733 cm^{-1}, C=O group vibration [26, 41, 63, 65, 66]. At 1615 cm^{-1} appears a band correspondent to the moisture of fibres [41, 56], although other authors attribute this peak to the presence of lignin [26, 67]. The band centred at 1506 cm^{-1} is attributed to lignin [41], and the

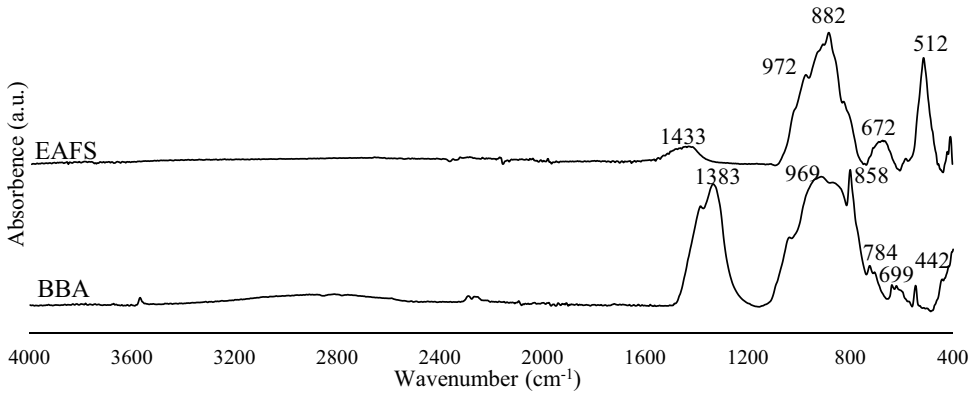

Fig. 11 ATR–FTIR spectra of precursors

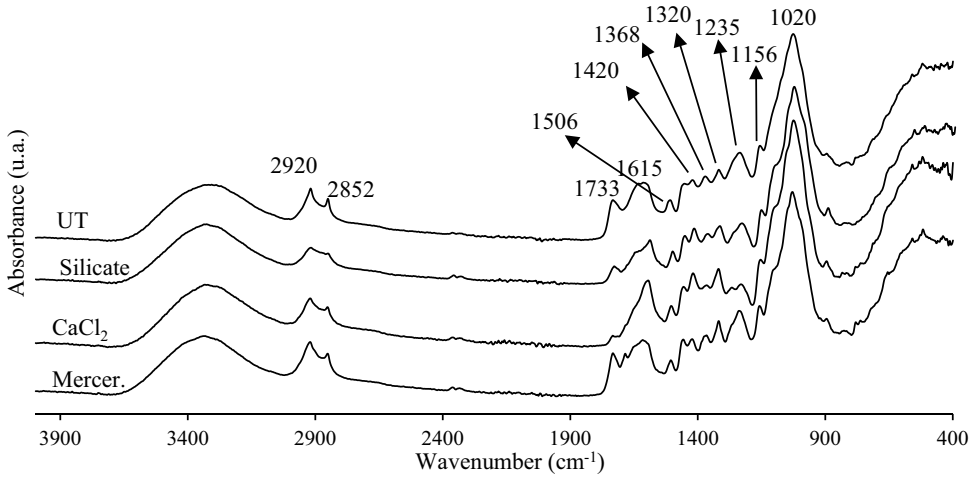

Fig. 12 FTIR spectra of olive-pruning fibres untreated and treated with different solutions

compound is also attributed to peaks centred at 1420, 1368 and 1320 cm^{-1}, according to Shahril et al. [68]. The peak centred at 1235 cm^{-1} is associated with lignin and hemicellulose compounds [56]. Cellulose is also attributed to peak centred at 1156 cm^{-1} [68]. The intense peak found at 1020 cm^{-1} is associated with cellulose [26, 63].

The infrared spectra of untreated and treated olive-pruning fibres (Fig. 12) reveal typical vibrational modes of natural fibre constituents such as cellulose, hemicellulose and lignin. These spectra show differences between them, presenting changes in intensities and wavenumbers. These changes are a consequence of chemical changes on the surface of fibres. The most significant changes are concentrated in specific areas of the spectra: 950–1800 and 2800–3000 cm^{-1}, according to other authors [56]. The band observed around 3400 cm^{-1} represents the –OH stretching vibration in the aromatic and aliphatic structure of the cellulosic fraction [69, 70]. The spectrum of the untreated fibre is characterized by the presence of two intense peaks at 2920 and 2850 cm^{-1}. These bands correspond to vibrations of the C–H asymmetric single bond in methylene groups [71], characteristic of lignocellulosic materials. These bands have less intensity after the mercerization process or when they are treated with silicate, which could be due to the release of hemicellulose from the fibres [56, 67]. The same behaviour is observed in the band centred at 1733 cm^{-1}, assigned to the vibration of non-aromatic carboxylic groups [72], which decreases its intensity with treatments. Applying a $CaCl_2$ solution to fibres, this band practically disappears. This behaviour is also due to the elimination of hemicellulose from the fibres, which is in agreement with other authors [67]. The bands centred at 1615 cm^{-1} are attributed to vibrations of C = C bonds of lignin, while those centred at 1506 and 1420 cm^{-1} are associated with aromatic skeletons, phenolic groups, which are attributed to asymmetric vibrations and deformations of the C–H group [73]. The band centred at 1250 cm^{-1} is associated with the vibration of the COO bonds of the acetyl groups of the hemicellulose [74]. All these bands (1615, 1506, 1420 and 1250 cm^{-1}) suffer a drop after the treatments, which shows the elimination of hemicellulose and lignin, since the structure of this compound is of a phenolic polymer [67]. Other characteristic bands of cellulosic components are found at 1320 and 1156 cm^{-1} associated with cellulosic alcoholic groups and the C–O–C stretching vibration of glycosidic rings, respectively [41, 75]. As for the intense band centred at 1020 cm^{-1}, it is attributed to the symmetric deformation of alkyl ethers and C–O–C ethers present [76], and its intensity decreases when fibres are subjected to the mercerization treatment, which shows that this treatment also releases part of the fibre cellulose. This behaviour can have negative aspects in the development of higher strength. Around 700–500 cm^{-1}, other bands appear, which are associated with in-plane and out-of-plane deformation vibrations of the aromatic ring [77].

After comparing the spectra of the untreated and treated fibres, it is determined that alkaline treatments (mercerization and sodium silicate treatment) are the ones that generate the greatest degradation on the surface of fibres, being higher in the treatment carried out with NaOH. Alkaline treatments manage to dissolve the lignin and hemicellulose of fibres, degrading the surface of the fibres and favouring fibre–matrix interaction, in addition to reducing the negative effects of the chemical nature of non-cellulosic compounds that can hinder matrix reactions in alkaline-activated cements [63]. This improvement in the union between both materials led to the development of greater mechanical resistance, as presented in the corresponding section. In addition, the residual sodium silicate from this treatment could contribute to a higher production of C–S–H gel [63].

3.6.3 Composite sample analysis

Binder manufactured: control paste and composites with fibres show similar FTIR spectra (Fig. 13). Besides, these spectra are similar to the FTIR spectra of BBA. Centred bands at 2900 and 1610 cm^{-1} as a consequence of hydration products are assigned to the stretching vibration modes of H–OH groups and the bending vibration O–H groups, respectively [78]. The band centred at 2900 cm^{-1} moves to higher values when fibres were treated with silicate. Bands assigned to CO_3^{-2} groups of $CaCO_3$ and $MgCO_3$ (1380–1469 cm^{-1}) [79] remain centred in the same position, varying their intensities, with greater absorption for control samples and M-1 and Sil-1-treated samples, which indicates a higher degree of carbonation of the specimens. Bands associated with Si–O–T bonds, centred at 950 cm^{-1} [80], suffer the same trend, where the highest absorptions were obtained for compositions M-1, Sil-1 and Sil-0.5. With respect to the control paste, there is a displacement in this band due to the addition of fibres. The displacement is caused by the overlap of the peak corresponding to cellulose in the treated and untreated fibres. Therefore, the displacement is less when fibres treated by mercerization are added, since this peak is less intense in this case.

The FTIR spectra for samples reinforced with 1% of sodium silicate as a function of curing time are shown in Fig. 14. The band associated with OH– bonds changes the position from 2870 to 3130 cm^{-1}, as curing time increases. This displacement to higher wavenumber is attributed to growth hydration products [80]. In addition, centred band at 1617 cm^{-1} increased the intensity with curing time, indicating more hydration products formed [81].

Alkali-activated cements reinforced with untreated fibres and treated fibres using different solutions show similar

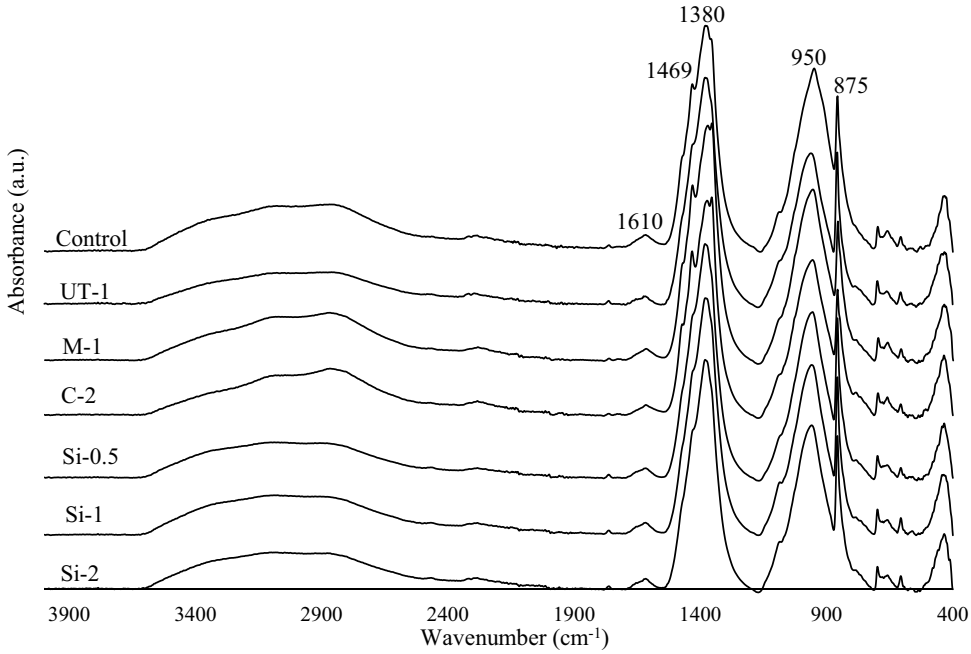

Fig. 13 FTIR spectra of control paste and composites reinforced with olive-pruning fibres at 28 days of curing

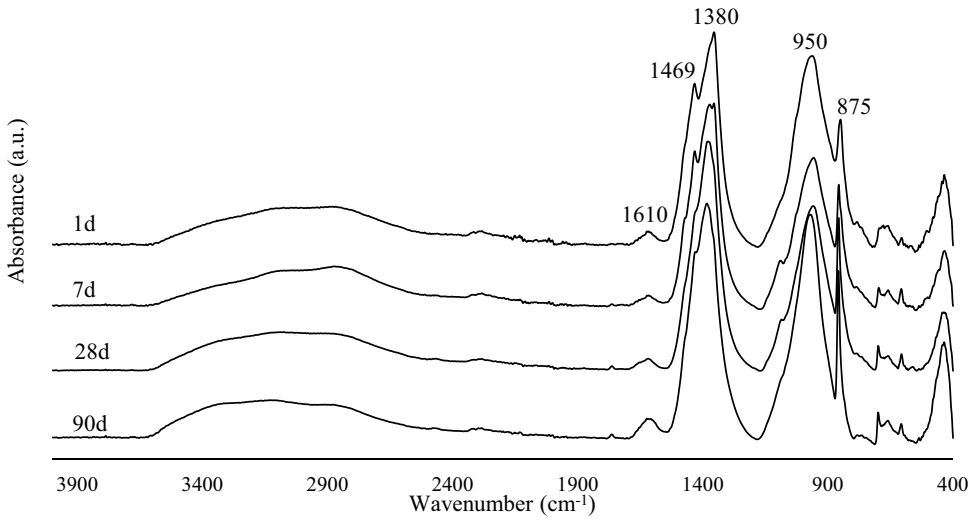

Fig. 14 ATR–FTIR of composites reinforced with 1% of fibre treatment with silicate, as a function of curing time

FTIR spectra to control paste. This indicates that the alkali activation matrix did not change significantly with the addition of olive-pruning fibres compared to control binder. Therefore, the combination of olive-pruning fibres with alkali-activated binder matrix could be mainly of a physical nature.

3.7 XRD analysis

The crystalline phases of precursors and composites were analysed by XRD. Diffractograms of precursors are shown in Fig. 15. Mainly merwinite ($CaMg(SiO_4)_2$) and gehlenite ($Ca_2Al_3SiO_7$) were found in EAFS, with traces of wuestite (FeO) and magnetite (FeO_2). In the case of BBA, quartz (SiO_2) was the main crystalline phase detected, with less quantities of calcite ($CaCO_3$), fairchildite ($K_2Ca(CO_3)_2$), lime (CaO) and potassium aluminosilicates ($KAlSiO_4$).

In Fig. 16, diffractograms of control paste and alkali-activated composites with 1 wt% of olive-pruning fibres untreated and treated with different solutions at 28 days of curing are shown. As just it was determined in previous works, diffractograms show a halo between 20 and 40° which indicates geopolymeric gel formation and no reactive phases in precursors such as quartz and calcite [29]. An increase of diffraction peak centred at 2-theta of 29.35° can be observed, associated with calcite. This peak increases in

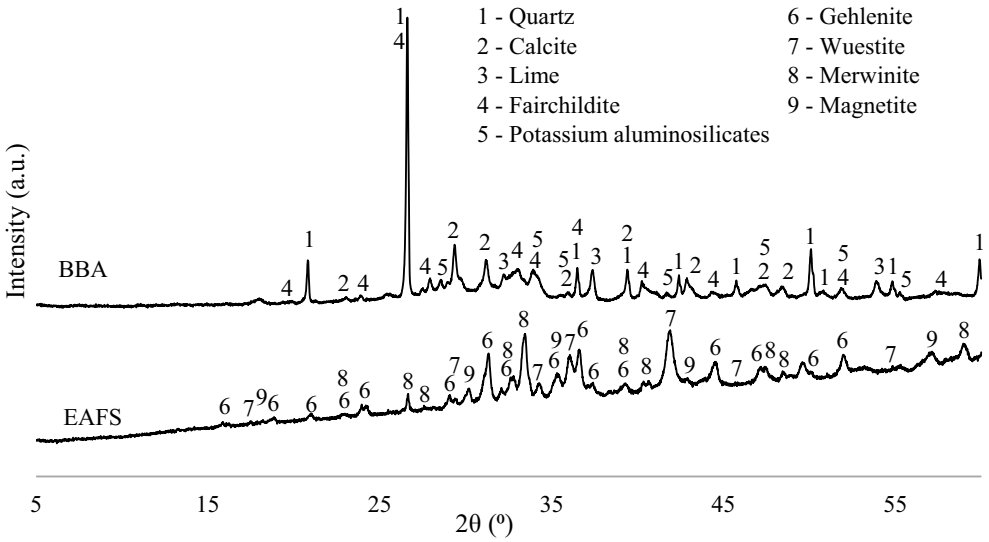

Fig. 15 XRD spectra of precursors

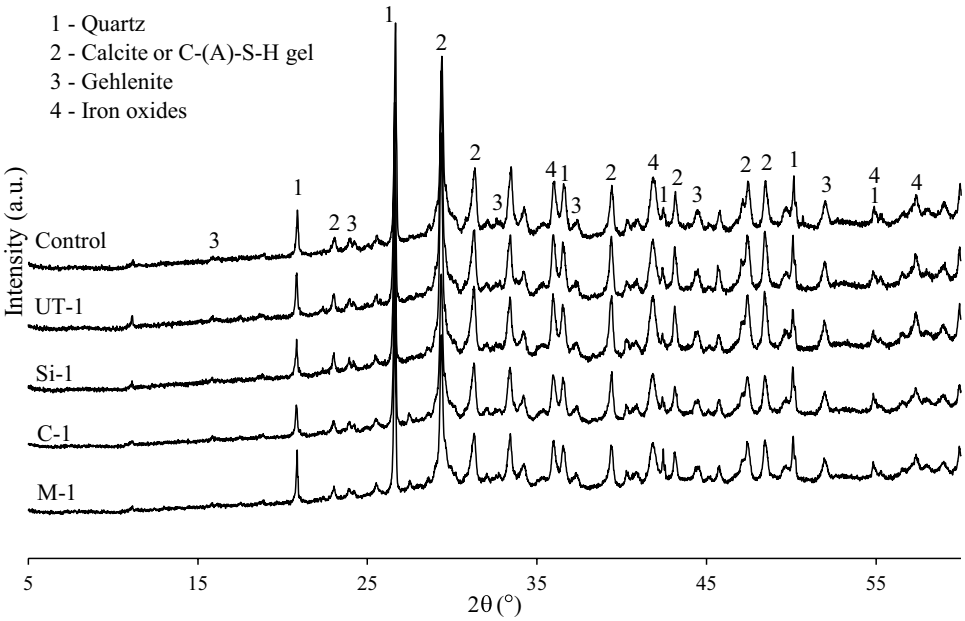

Fig. 16 XRD spectra of control paste and composites reinforced with 1 wt% of olive-pruning fibres

control paste and composites with fibres, indicating a carbonation of the matrix.

No significant changes are seen when fibres are added as reinforcement, and new crystalline phases are not formed, which means that fibres do not contribute to changes in the matrix structure.

3.8 Microstructural analysis

Micrographs of the control samples and composites reinforced with olive-pruning fibres after 28 days of curing are shown in Fig. 17. The control sample presents a compact appearance, due to the formation of the C–(A)–S–H gel (spectrum 1) together with the formation of geopolymeric gel (C,K)–(A)–S–H (spectrum 2). In addition, some unreacted particles (spectrum 3), as well as the appearance of microcracks produced by the evaporation of water in the geopolymeric reactions during the curing time, are observed [29]. The matrix of the manufactured alkaline-activated cements does not show significant changes in its microstructure when fibres are added (Fig. 18). Fibre-reinforced cements also present microcracks, which are less abundant when lower fibre contents are used, with Sil-0.5 (Fig. 18f), since the fibres can be better distributed. With higher fibre

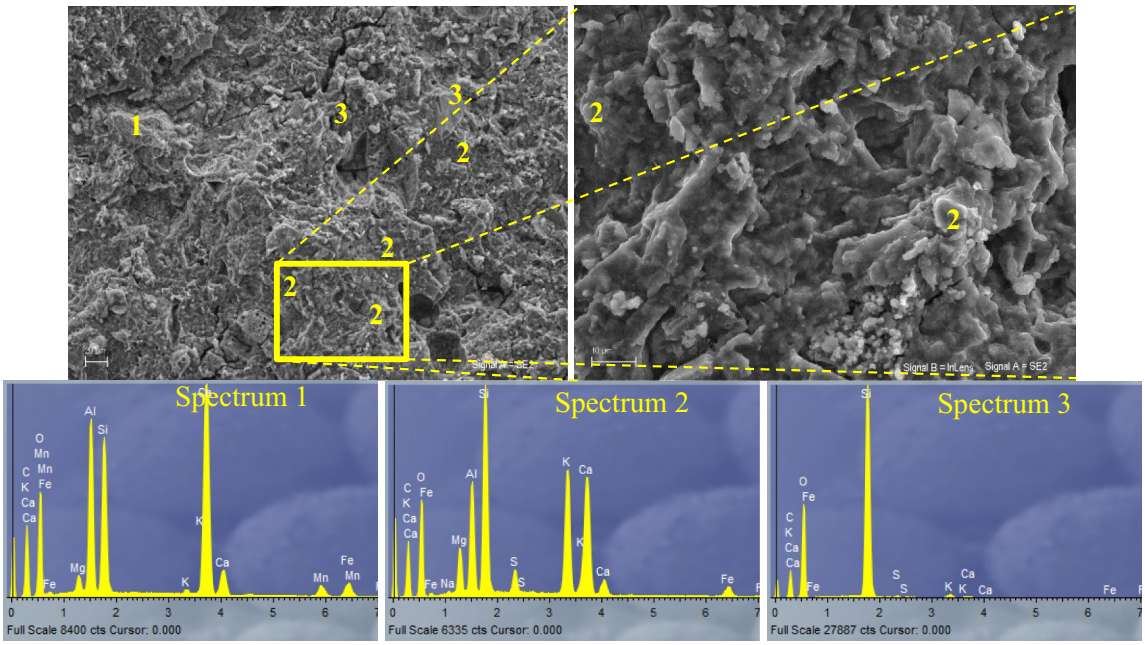

Fig. 17 Matrix details in control sample at 28 days of curing

content, greater agglomerations are produced, reducing workability and worse fibre distribution, causing the appearance of larger cracks in the matrix [82].

Fibres added for reinforcement can break, stretch or pull out of the matrix under applied loads [82]. It can be observed from all the samples that how the fibres break or pull out of the matrix. In the case of pull-out, more energy is spent in the development of cracks, that is the fibres absorb that energy, with which composites have a more ductile behaviour [82]. This detachment leaves traces in the matrix, as a sign of the adhesion between fibre and matrix, hence the ability to dissipate energy and increase its fracture toughness [83]. The detachment can occur with or without matrix material deposition. In the case of containing adhered material from the matrix, it suggests a good union between fibre and matrix [18]. This was observed in the fibres treated with NaOH, while in untreated fibres, this deposit is barely noticeable in the pulled-out fibres, a sign of less adherence. In the case of the fibres treated with $CaCl_2$ and silicate, no pull-out fibres were observed, but it can be seen how the fibres are tightly wrapped by the matrix, indicating a high degree of adhesion between the fibre and matrix. This behaviour is also observed in fibre-reinforced composites treated with NaOH, with which for these specimens pull-out fibres were found with a tight bond with the matrix.

The good adhesion of the fibre with the matrix is due to the contact surface of the fibres, as well as to the precipitation of the alkaline cement in the exposed cavities of the fibre and the union between the cellulose chain of treated fibres and calcium-based hydration products from alkali-activated cements [25]. Moisture absorbed in the fibres is released into the matrix over time, which can lead to increased matrix hydration, leading to higher gel content [11]. This release of moisture produces a contraction of the fibre, leaving voids between the fibre and the matrix, which can be partially filled with the hydration products [11]. This behaviour is due to the cellulose hydroxyl that increases the absorption capacity of the fibres, and according to some authors, it could be used as a method of internal repair in cementitious materials, helping to reduce crack propagation during curing time [13].

The SEM images of untreated and treated fibres are shown in Fig. 19. The surface differences between untreated and treated fibres are significant. The untreated fibres have a smooth surface, while the treated ones have a rougher surface. The roughness of the fibres can be increased by removing wax and other impurities present in the raw fibre, thus creating a rough surface with voids, which increases the contact area between the matrix and the fibre [8, 13]. Treatments used in this study on olive-pruning fibres managed to eliminate these impurities, but also removed part of the lignin and hemicellulose from the fibres (as shown in the FTIR analysis), achieving greater wear on the surface, making it more open and rough, thereby increasing the contact area [16, 25, 66]. This higher surface roughness means better fibre–matrix

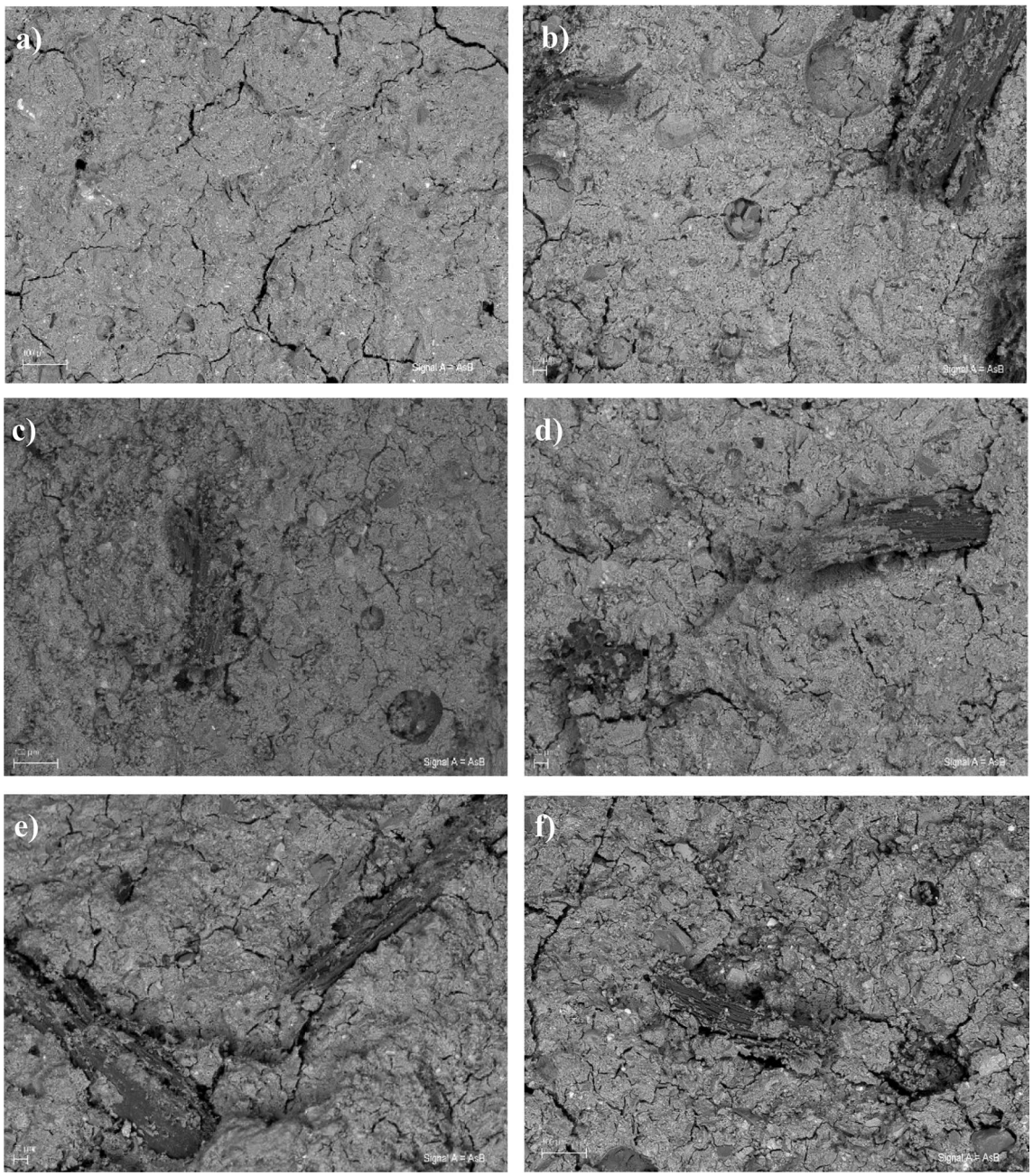

Fig. 18 Backscattered SEM images of composites manufactured: **a** control paste, **b** reinforced with 1 wt% untreated fibres, **c** reinforced with 1 wt% fibres treated by $CaCl_2$ solution, **d** reinforced with 1 wt% fibres treated by mercerization method, **e** and **f** reinforced with 1 and 0.5 wt% fibres treated by sodium silicate solution, respectively

interaction. By increasing the friction between both components, the ability to resist shear and bending forces is increased [41, 84]. In addition, treatments on the fibres can improve the crystallinity of the cellulose and shorten the spacing between the cellulose chains, improving the strength of the fibre [24]. For all this, there is an increase in mechanical strength.

SEM images also reveal the existence of cavities with different shapes and sizes inside the fibres. In treated fibres, it becomes more evident due to degradation of the

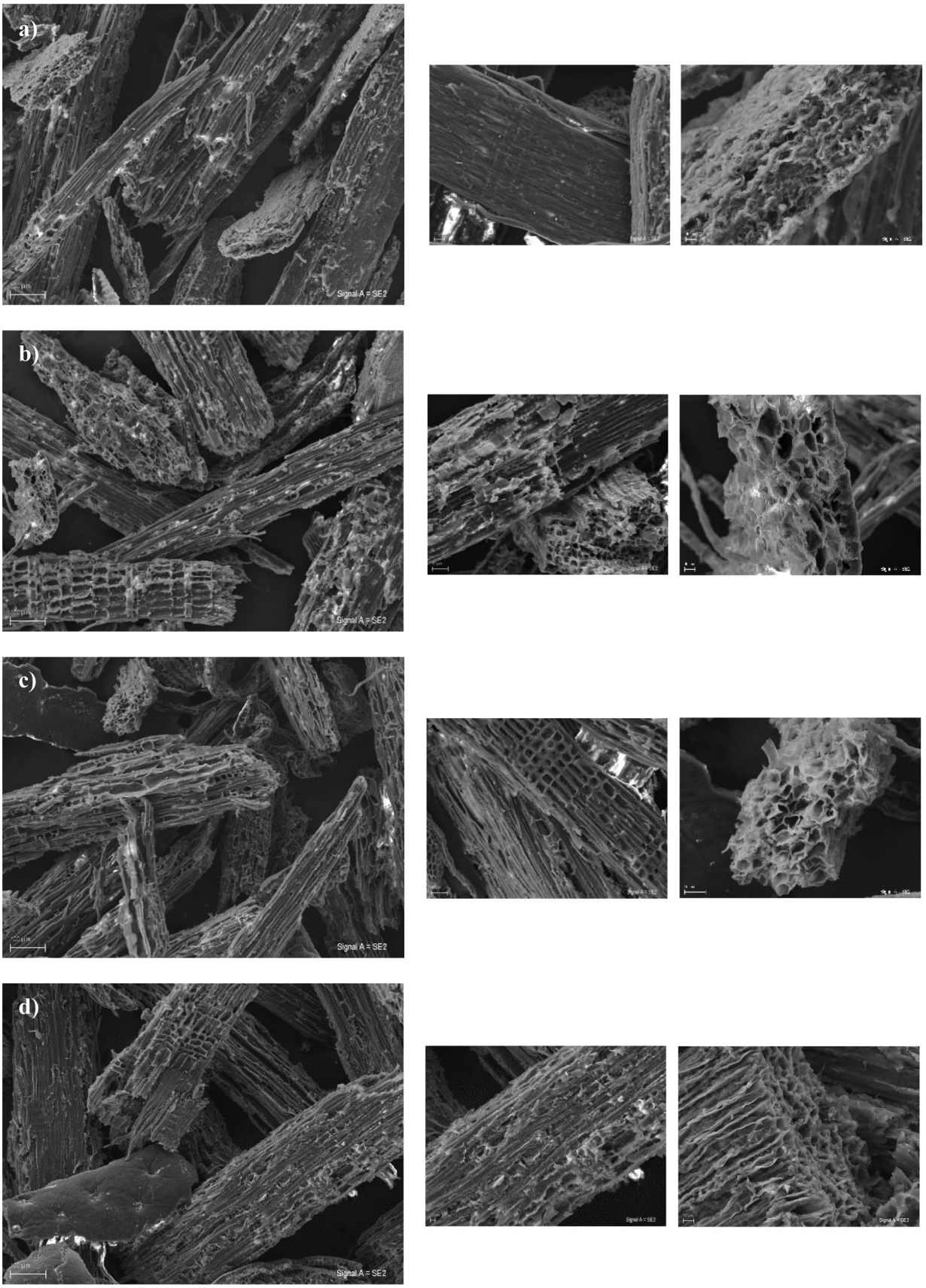
a)
b)
c)
d)
Signal A = SE2

◂**Fig. 19** General SEM images (100×), longitudinal (250×) and cross-Sect. (500×) of untreated and treated olive-pruning fibres: **a** untreated fibres, **b** fibres treated with $CaCl_2$ solution, **c** fibres treated by mercerization process, and **d** fibres treated with sodium silicate solution

outermost surface of the fibre. These internal cavities contribute to the increase in the water absorption of the matrix [11], as already determined in the physical properties of the composites.

The EDS analysis developed over treated and untreated fibre surfaces (Table 3) shows that C/O ratio decreases on applying treatments. This indicates the disappearance of lignin and cellulose in fibres. In addition, the presence of Ca, Na and Si deposits was detected, which are from treatment solutions, in the fibre surfaces [62].

4 Conclusion

In the present study, the technological properties of alkali-activated cement composites based on electric arc furnace and biomass bottom ash reinforcement with alkali-treated and -untreated olive-pruning fibres (0.5–2 wt%) were checked. The fibres were subjected to three different treatments: 10 wt% Na_2SiO_3 solution, 3 wt% $CaCl_2$ solution and 5 wt% NaOH solution with the primary aim of improving the flexural strength and toughness of the manufactured material. Experimental results showed that the flexural strength of composites improved (up to 20%) and promoted a less fragile failure, due to the ability to transfer stress from matrix to fibres. The improvement in flexural strength is mainly due to the degradation of fibre surface, achieving better fibre–matrix adhesion. All treatments used in this research degraded the surface of fibres, removing much of lignin, cellulose and hemicellulose to a greater or lesser extent. In addition, the moisture present in fibres can react with residual activating solution and they can fill spaces in the matrix or between matrix and fibre, and thus improve the properties of composites. The optimal percentage for reinforcement obtained was 1 wt%. The best treatment option for fibres was using a solution of 10 wt% Na_2SiO_3. In the case of fibres treated with sodium silicate, the residual treatment solution deposited on fibre surface helped to produce a denser and stronger matrix. Although a solution of 5% NaOH (mercerization) or 3 wt% $CaCl_2$ also obtained good results. Composites reinforcement improved values of control paste in a 20.1% and 20% for untreated fibres, when 1% of fibres were used.

Thermal conductivity using fibres as reinforcement in binders decreased with the amount of fibres and has a better thermal insulation capacity. The best results were obtained for composites with 2 wt% of untreated fibres and mercerization-treated fibres in accordance with its higher apparent porosity.

In summary, the results indicate that olive-pruning fibres can be a reinforcement for binders manufactured from electric arc furnace and biomass bottom ash. Employing optimal treatment and using optimal amount, composites with higher flexural strength, ductility and insulation capacity can be obtained, presenting similar compressive strength and physical properties (bulk density, apparent porosity and water absorption) as the control cement. The mechanical strength results indicate that the composites present adequate values to be used as non-structural materials, according to the properties of isolated materials.

Table 3 EDS analysis of untreated and treated olive-pruning fibre surfaces

Treatment	C	O	Ca	Na	Si	C/O
UT	68.58	29.07	0.84	–	–	2.36
	65.36	31.7	0.68	–	–	2.06
10% Na_2SiO_3	49.52	29.61	1.83	0.42	1.41	1.67
	61.22	36.39	0.71	0.97	0.71	1.68
3% $CaCl_2$	51.43	40.43	8.15	–	–	1.27
	53.74	41.23	7.42	–	–	1.30
5% NaOH	51	42.64	3.31	2.84	–	1.20
	54.1	39.08	3.75	2.81	–	1.38

Acknowledgements This work has been funded by the project PID2020-115161RB-I00: Applying the circular economy in the development of new low carbon footprint alkaline activated hydraulic binders for construction solutions (CongActiva), MCIN/AEI/https://doi.org/10.13039/501100011033 FEDER 'A way of making Europe and by the project MAT2017-88097-R: Development and characterization of new geopolymeric composites based on waste from the olive industry. Towards a sustainable construction, FEDER/Ministry of Science, Innovation and Universities, State Research Agency'. The authors thank Siderúrgica Sevillana company and Aldebarán Energía del Guadalquivir company for supplying slag and ash, respectively. M.A. Gómez-Casero acknowledges support of MINECO (PRE2018-084073). Technical and human support provided by CICT of Universidad de Jaén (UJA, MINECO, Junta de Andalucía, FEDER) is gratefully acknowledged.

Author contributions MAG-C: conceptualization; data curation; methodology; formal analysis and investigation; writing—original draft preparation and writing—review and editing. PJS-S: writing—review and editing. EC: writing—review and editing; resources and supervision. DE-Q: resources; supervision; funding acquisition and writing—review and editing.

Funding Funding for open access publishing: Universidad de Jaén/CBUA.

Declarations

Conflict of interest This work was supported by the Ministry of Science, Innovation and Universities (Grant numbers: MAT2017-88097-R, PRE2018-084073 and ID2020-115161RB-I00). The authors declare that they have no known competing financial interests or personal relationships that could have appeared to influence the work reported in this paper.

Ethical approval The manuscript has not been submitted (partly or in full) to another journal for simultaneous consideration during the editorial review process.

References

1. Provis JL. Geopolymers and other alkali activated materials: Why, how, and what? Mater Struct. 2014;47:11–25.
2. Gómez-Casero MA, Moral-Moral FJ, Pérez-Villarejo L, Sánchez-Soto PJ, Eliche-Quesada D. Synthesis of clay geopolymers using olive pomace fly ash as an alternative activator. Influence of the additional commercial alkaline activator used. J Market Res. 2021;12:1762–76.
3. Pliatsikas I, Robou E, Samouhos M, Katsiotis NS, Tsakiridis PE. Valorization of demolition ceramic wastes and lignite bottom ash for the production of ternary blended cements. Constr Build Mater. 2019;229:116879.
4. Nawaz M, Heitor A, Sivakumar M. Geopolymers in construction-recent developments. Constr Build Mater. 2020;260:120472. https://doi.org/10.1016/j.conbuildmat.2020.120472.
5. Al-Rousan ET, Khalid HR, Rahman MK. Fresh, mechanical, and durability properties of basalt fiber-reinforced concrete (BFRC): a review. Dev Built Environ. 2023. https://doi.org/10.1016/j.dibe.2023.100155.
6. Stapper JL, Gauvin F, Brouwers HJH. Influence of short-term degradation on coir in natural fibre-cement composites. Constr Build Mater. 2021;306:124906. https://doi.org/10.1016/j.conbuildmat.2021.124906.
7. Long WJ, Wu Z, Khayat KH, Wei J, Dong B, Xing F, Zhang J. Design, dynamic performance and ecological efficiency of fiber-reinforced mortars with different binder systems: ordinary Portland cement, limestone calcined clay cement and alkali-activated slag. J Clean Prod. 2022;337:130478.
8. de Souza Castoldi R, de Souza LMS, Souto F, Liebscher M, Mechtcherine V, de Andrade Silva F. Effect of alkali treatment on physical–chemical properties of sisal fibers and adhesion towards cement-based matrices. Constr Build Mater. 2022;345:128363.
9. Amran M, Fediuk R, Abdelgader HS, Murali G, Ozbakkaloglu T, Lee YH, Lee YY. Fiber-reinforced alkali-activated concrete: a review. J Build Eng. 2022;45:103638.
10. Silva G, Kim S, Aguilar R, Nakamatsu J. Natural fibers as reinforcement additives for geopolymers—a review of potential eco-friendly applications to the construction industry. Sustain Mater Technol. 2020;23:e00132.
11. Choi YC. Hydration and internal curing properties of plant-based natural fiber-reinforced cement composites. Case Stud Constr Mater. 2022;17:e01690.
12. Ardanuy M, Claramunt J, Toledo Filho RD. Cellulosic fiber reinforced cement-based composites: a review of recent research. Constr Build Mater. 2015;79:115–28.
13. Lee GW, Choi YC. Effect of abaca natural fiber on the setting behavior and autogenous shrinkage of cement composite. J Build Eng. 2022;56:104719.
14. Feng B, Liu J, Lu Z, Zhang M, Tan X. Study on properties and durability of alkali activated rice straw fibers cement composites. J Build Eng. 2023;63:105515. https://doi.org/10.1016/j.jobe.2022.105515.
15. Claramunt J, Ardanuy M, García-Hortal JA, Tolêdo Filho RD. The hornification of vegetable fibers to improve the durability of cement mortar composites. Cem Concr Compos. 2011;33(5):586–95.
16. Zhou F, Cheng G, Jiang B. Effect of silane treatment on microstructure of sisal fibers. Appl Surf Sci. 2014;292:806–12.
17. Asim M, Jawaid M, Abdan K, Ishak MR. Effect of alkali and silane treatments on mechanical and fibre-matrix bond strength of kenaf and pineapple leaf fibres. J Bionic Eng. 2016;13(3):426–35.
18. Orue A, Jauregi A, Unsuain U, Labidi J, Eceiza A, Arbelaiz A. The effect of alkaline and silane treatments on mechanical properties and breakage of sisal fibers and poly (lactic acid)/sisal fiber composites. Compos A Appl Sci Manuf. 2016;84:186–95. https://doi.org/10.1016/j.compositesa.2016.01.021.
19. Zahari WZW, Badri RNRL, Ardyananta H, Kurniawan D, Nor FM. Mechanical properties and water absorption behavior of polypropylene/ijuk fiber composite by using silane treatment. Procedia Manuf. 2015;2:573–8.
20. Santana HA, Júnior NSA, Ribeiro DV, Cilla MS, Dias CM. Vegetable fibers behavior in geopolymers and alkali-activated cement based matrices: a review. J Build Eng. 2021;44:103291.

21. Ouarhim W, Zari N, Bouhfid R. Mechanical performance of natural fibers–based thermosetting composites. In: Jawaid M, Thariq M, Saba N, editors. Mechanical and physical testing of biocomposites, fibre-reinforced composites and hybrid composites. Sawston: Woodhead Publishing; 2019. p. 43–60.
22. Mohammed M, Rahman R, Mohammed AM, Adam T, Betar BO, Osman AF, Dahham OS. Surface treatment to improve water repellence and compatibility of natural fiber with polymer matrix: recent advancement. Polym Test. 2022. https://doi.org/10.1016/j.polymertesting.2022.107707.
23. Sanchez-Echeverri LA, Ganjian E, Medina-Perilla JA, Quintana GC, Sanchez-Toro JH, Tyrer M. Mechanical refining combined with chemical treatment for the processing of Bamboo fibres to produce efficient cement composites. Constr Build Mater. 2021;269:121232.
24. Islam MH, Islam MR, Dulal M, Afroj S, Karim N. The effect of surface treatments and graphene-based modifications on mechanical properties of natural jute fiber composites: a review. iScience. 2022;25(1):103597.
25. Li M, Zhou S, Guo X. Effects of alkali-treated bamboo fibers on the morphology and mechanical properties of oil well cement. Constr Build Mater. 2017;150:619–25. https://doi.org/10.1016/j.conbuildmat.2017.05.215.
26. Akinyemi AB, Omoniyi ET, Onuzulike G. Effect of microwave assisted alkali pretreatment and other pretreatment methods on some properties of bamboo fibre reinforced cement composites. Constr Build Mater. 2020;245:118405. https://doi.org/10.1016/j.conbuildmat.2020.118405.
27. Dhasindrakrishna K, Pasupathy K, Ramakrishnan S, Sanjayan J. The ambient and elevated temperature performance of hemp fibre reinforced alkali-activated cement foam: effects of fibre dosage and alkali treatment. J Build Eng. 2023. https://doi.org/10.1016/j.jobe.2023.107131.
28. Fei M, Fu W, Zheng X, Chen Y, Liu W, Qiu R. Enhancing cement composite interface with waterglass modification on bamboo fiber: a viable and effective approach. Constr Build Mater. 2024;411:134338.
29. Gómez-Casero MA, Pérez-Villarejo L, Castro E, Eliche-Quesada D. Effect of steel slag and curing temperature on the improvement in technological properties of biomass bottom ash based alkali-activated materials. Constr Build Mater. 2021;302:124205. https://doi.org/10.1016/j.conbuildmat.2021.124205.
30. Qian C, Yi H, Du W. Bacteria fixing CO_2 to enhance the volume stability of ground steel slag powder as a component of cement-based materials aiming at clean production. J Clean Prod. 2021;314:127821.
31. Padilla-Rascón C, Carvalheiro F, Duarte LC, Roseiro LB, Ruiz E, Castro E. An integrated olive stone biorefinery based on a two-step fractionation strategy. Ind Crops Prod. 2022;187:115157. https://doi.org/10.1016/j.indcrop.2022.115157.
32. Sluiter A, Hames B, Ruiz R, Scarlata C, Sluiter J, Templeton D, Crocker D. Determination of structural carbohydrates and lignin in biomass. Golden: National Renewable Energy Laboratory; 2012.
33. UNE-EN 1015-11:2000/A1:2007. Methods of test for mortar for masonry – part 11: determination of flexural and compressive strength of hardened mortar. 2007
34. UNE-EN 1015-10:2000. Methods of test for mortar for masonry - part 10: determination of dry bulk density of hardened mortar. 2000
35. ISO-8302,1991. Thermal insulation—determination of steady-state thermal resistance and related properties—guarded hot plate apparatus. 1991
36. ASTM C230/C230M-14. Standard specification for flow table for use in tests of hydraulic cement. West Conshohocken: ASTM International; 2014.
37. Luo T, Yuan H, Wang Q. Comparison the properties of carbon fiber-based Portland cement and alkali-activated fly ash/slag conductive cementitious composites. J Build Eng. 2023;76:107134. https://doi.org/10.1016/j.jobe.2023.107134.
38. Saba AM, Khan AH, Akhtar MN, Khan NA, Koloor SSR, Petrů M, Radwan N. Strength and flexural behavior of steel fiber and silica fume incorporated self-compacting concrete. J Market Res. 2021;12:1380–90. https://doi.org/10.1016/j.jmrt.2021.03.066.
39. Guler S, Akbulut ZF. Workability, physical and mechanical properties of the cement mortars strengthened with metakaolin and steel/basalt fibers exposed to freezing-thawing periods. Constr Build Mater. 2023;394:132100. https://doi.org/10.1016/j.conbuildmat.2023.132100.
40. Yan L, Chouw N, Yuan X. Improving the mechanical properties of natural fibre fabric reinforced epoxy composites by alkali treatment. Reinf Plast Compos. 2012;31(6):425–37. https://doi.org/10.1177/0731684412439494.
41. Malenab RAJ, Ngo JPS, Promentilla MAB. Chemical treatment of waste abaca for natural fiber-reinforced geopolymer composite. Materials. 2017;10(6):579. https://doi.org/10.3390/ma10060579.
42. Huang Y, Tan J, Xuan X, Liu L, Xie M, Liu H, Shujuan Yu, Zheng G. Study on untreated and alkali treated rice straw reinforced geopolymer composites. Mater Chem Phys. 2021;262(1):124304. https://doi.org/10.1016/j.matchemphys.2021.124304.
43. Alomayri T, Low IM. Synthesis and characterization of mechanical properties in cotton fiber-reinforced geopolymer composites. J Asian Ceram Soc. 2013;1(1):30–4.
44. Alomayri T. Effect of glass microfibre addition on the mechanical performances of fly ash-based geopolymer composites. J Asian Ceram Soc. 2017;5(3):334–40.
45. Alomayri T, Shaikh FUA, Low IM. Characterisation of cotton fibre-reinforced geopolymer composites. Compos B Eng. 2013;50:1–6. https://doi.org/10.1016/j.compositesb.2013.01.013.
46. Talimi M, Rizvi G. Properties enhancement of PLA-natural fibre composites using an ethylene copolymer. World J Eng. 2008;20(26):1461–2.
47. Wongsa A, Kunthawatwong R, Naenudon S, Sata V, Chindaprasirt P. Natural fiber reinforced high calcium fly ash geopolymer mortar. Constr Build Mater. 2020;241:118143.
48. Poletanovic B, Dragas J, Ignjatovic I, Komljenovic M, Merta I. Physical and mechanical properties of hemp fibre reinforced alkali-activated fly ash and fly ash/slag mortars. Constr Build Mater. 2020;259:119677.
49. Silva G, Kim S, Bertolotti B, Nakamatsu J, Aguilar R. Optimization of a reinforced geopolymer composite using natural fibers and construction wastes. Constr Build Mater. 2020;258:119697.
50. Azevedo AR, Lima TE, Reis RH, Oliveira MS, Candido VS, Monteiro SN. Guaruman fiber: a promising reinforcement for cement-based mortars. Case Stud Constr Mater. 2022;16:e01029.
51. Neithalath N, Weiss J, Olek J. Acoustic performance and damping behavior of cellulose–cement composites. Cement Concr Compos. 2004;26(4):359–70.
52. Ramakrishna, G. (2022). Oil Palm Empty Fruit Bunch Fiber Surface Morphology, Treatment, And Suitability As Reinforcement In Cement Composites: A State Of The Art Review. Cleaner Materials, 100144
53. Nkwaju RY, Djobo JNY, Nouping JNF, Huisken PWM, Deutou JGN, Courard LJACS. Iron-rich laterite-bagasse fibers based geopolymer composite: mechanical, durability and insulating properties. Appl Clay Sci. 2019;183:105333.
54. Ravindran D, Sundara Bharathi SR, Indran S. Characterization of surface-modified natural cellulosic fiber extracted from the root of *Ficus religiosa* tree. Int J Biol Macromol.

2020;156:997–1006. https://doi.org/10.1016/j.ijbiomac.2020.04.117.
55. Lazorenko G, Kasprzhitskii A, Kruglikov A, Mischinenko V, Yavna V. Sustainable geopolymer composites reinforced with flax tows. Ceram Int. 2020;46(8):12870–5. https://doi.org/10.1016/j.ceramint.2020.01.184.
56. Lazorenko G, Kasprzhitskii A, Yavna V, Mischinenko V, Kukharskii A, Kruglikov A, et al. Effect of pre-treatment of flax tows on mechanical properties and microstructure of natural fiber reinforced geopolymer composites. Environ Technol Innov. 2020;20:101105. https://doi.org/10.1016/j.eti.2020.101105.
57. Kamble AD, Mendhe VA, Chavan PD, Saxena VK. Insights of mineral catalytic effects of high ash coal on carbon conversion in fluidized bed Co-gasification through FTIR, XRD, XRF and FE-SEM. Renewable Energy. 2022;183:729–51.
58. Rafeet A, Vinai R, Soutsos M, Sha W. Effects of slag substitution on physical and mechanical properties of fly ash-based alkali activated binders (AABs). Cem Concr Res. 2019;122:118–35.
59. Ke X, Baki VA, Skevi L. Mechanochemical activation for improving the direct mineral carbonation efficiency and capacity of a timber biomass ash. J CO2 Util. 2023;68:102367.
60. Adediran A, Yliniemi J, Lemougna PN, Perumal P, Illikainen M. Recycling high volume Fe-rich fayalite slag in blended alkali-activated materials: effect of ladle and blast furnace slags on the fresh and hardened state properties. J Build Eng. 2023;63:105436.
61. Yaseri S, Verki VM, Mahdikhani M. Utilization of high volume cement kiln dust and rice husk ash in the production of sustainable geopolymer. J Clean Prod. 2019;230:592–602.
62. Tiwari YM, Sarangi SK. Characterization of raw and alkali treated cellulosic Grewia Flavescens natural fiber. Int J Biol Macromol. 2022;209:1933–42. https://doi.org/10.1016/j.ijbiomac.2022.04.169.
63. Ntimugura F, Wilson K, Vinai R, Walker P. Effect of alkali-silica treatments of miscanthus fibres on chemical and micro-morphological modifications. Clean Mater. 2023. https://doi.org/10.1016/j.clema.2023.100182.
64. Dash C, Bisoyi DK. Microwave radiation technique for the isolation of Sunn Hemp natural fiber in the application of material processing. J Non-Cryst Solids. 2022;591:121706. https://doi.org/10.1016/j.jnoncrysol.2022.121706.
65. Lobregas MOS, Buniao EVD, Leaño JL. Alkali-enzymatic treatment of *Bambusa blumeana* textile fibers for natural fiber-based textile material production. Ind Crops Prod. 2023;194:116268. https://doi.org/10.1016/j.indcrop.2023.116268.
66. Kundu SP, Chakraborty S, Majumder SB, Adhikari B. Effectiveness of the mild alkali and dilute polymer modification in controlling the durability of jute fibre in alkaline cement medium. Constr Build Mater. 2018;174:330–42. https://doi.org/10.1016/j.conbuildmat.2018.04.134.
67. Iskandar WME, Ong HR, Khan MMR, Ramli R. Effect of ultrasonication on alkaline treatment of empty fruit bunch fibre: Fourier transform infrared spectroscopy (FTIR) and morphology study. Mater Today Proc. 2022;66:2840–3. https://doi.org/10.1016/j.matpr.2022.06.526.
68. Shahril SM, Ridzuan MJM, Majid MA, Bariah AMN, Rahman MTA, Narayanasamy P. Alkali treatment influence on cellulosic fiber from *Furcraea foetida* leaves as potential reinforcement of polymeric composites. J Mater Res Technol. 2022;19:2567–83. https://doi.org/10.1016/j.jmrt.2022.06.002.
69. Asimbaya C, Rosas N, Endara D, Guerrero V. Obtención de Carbón Activado a partir de Residuos Lignocelulósicos de Canelo, Laurel y Eucalipto. Revista Politécnica. 2015;36(3):24.
70. Kumar A, Gupta V, Gaikwad KK. Microfibrillated cellulose from pine cone: extraction, properties, and characterization. Biomass Convers Biorefinery. 2021;13:1–8.
71. Özçimen D, Ersoy-Meriçboyu A. Adsorption of copper(II) ions onto hazelnut shell and apricot stone activated carbons. Adsorpt Sci Technol. 2010. https://doi.org/10.1260/0263-6174.28.4.327.
72. Macias-Garcia A, Gomez Corzo M, Alfaro Dominguez M, Alexandre Franco M, Martinez Naharro J. Study of the adsorption and electroadsorption process of Cu (II) ions within thermally and chemically modified activated carbon. J Hazard Mater. 2017;328:46–55. https://doi.org/10.1016/j.jhazmat.2016.11.036.
73. Li S, Han K, Li J, Li M, Lu C. Preparation and characterization of super activated carbon produced from gulfweed by KOH activation. Microporous Mesoporous Mater. 2017;243:291–300. https://doi.org/10.1016/j.micromeso.2017.02.052.
74. da Silva SPM, da Costa Lopes AM, Roseiro LB, Bogel-Łukasik R. Novel pre-treatment and fractionation method for lignocellulosic biomass using ionic liquids. RSC Adv. 2013;3:16040–50.
75. Arrakhiz FZ, El Achaby M, Benmoussa K, Bouhfid R, Essassi EM, Qaiss A. Evaluation of mechanical and thermal properties of Pine cone fibers reinforced compatibilized polypropylene. Mater Des. 2012;40:528–35.
76. Morosanu I, Teodosiu C, Paduraru C, Ibanescu D, Tofan L. Biosorption of lead ions from aqueous effluents by rapeseed biomass. New Biotechnol. 2017;39:110–24. https://doi.org/10.1016/j.nbt.2016.08.002.
77. Yorgun S, Yıldız D. Slow pyrolysis of paulownia wood: effects of pyrolysis parameters on product yields and bio-oil characterization. J Anal Appl Pyrolysis. 2015;114:68–78. https://doi.org/10.1016/j.jaap.2015.05.003.
78. Ismail I, Bernal SA, Provis JL, San Nicolas R, Hamdan S, van Deventer JS. Modification of phase evolution in alkali-activated blast furnace slag by the incorporation of fly ash. Cement Concr Compos. 2014;45:125–35.
79. Ye N, Yang J, Liang S, Hu Y, Hu J, Xiao B, Huang Q. Synthesis and strength optimization of one-part geopolymer based on red mud. Constr Build Mater. 2016;111:317–25.
80. Lemougna PN, Wang KT, Tang Q, Cui XM. Synthesis and characterization of low temperature (< 800 C) ceramics from red mud geopolymer precursor. Constr Build Mater. 2017;131:564–73.
81. Gómez-Casero MA, Pérez-Villarejo L, Sánchez-Soto PJ, Eliche-Quesada D. Comparative study of alkali activated cements based on metallurgical slags, in terms of technological properties developed. Sustain Chem Pharm. 2022;29:100746. https://doi.org/10.1016/j.scp.2022.100746.
82. Haily E, Zari N, Bouhfid R, Qaiss A. Natural fibers as an alternative to synthetic fibers in the reinforcement of phosphate sludge-based geopolymer mortar. J Build Eng. 2023;67:105947. https://doi.org/10.1016/j.jobe.2023.105947.
83. Bayraktar OY, Tobbala DE, Turkoglu M, Kaplan G, Tayeh BA. Hemp fiber reinforced one-part alkali-activated composites with expanded perlite: mechanical properties, microstructure analysis and high-temperature resistance. Constr Build Mater. 2023;363:129716. https://doi.org/10.1016/j.conbuildmat.2022.129716.
84. Ding L, Han X, Cao L, Chen Y, Ling Z, Han J, et al. Characterization of natural fiber from manau rattan (*Calamus manan*) as a potential reinforcement for polymer-based composites. J Bioresour Bioprod. 2022;7(3):190–200. https://doi.org/10.1016/j.jobab.2021.11.002.